Electron microscope investigations of activated chalcopyrite particles via the FLSmidth® ROL process

Karcz, Adam Paul; Damø, Anne Juul; Illerup, Jytte Boll; Rocks, Sara; Dam-Johansen, Kim; Chaiko, David

Published in:
Journal of Materials Science

Link to article, DOI:
10.1007/s10853-017-1308-y

Publication date:
2017

Document Version
Peer reviewed version

Adam Paul Karcz[1,*], Anne Juul Damø[1], Jytte Boll Illerup[1], Sara Rocks[2], Kim Dam-Johansen[1], and David Chaiko[2]

[1] Department of Chemical and Biochemical Engineering, Danmarks Tekniske Universitet, Søltofts Plads, Building 229, 2800 Kongens Lyngby, Denmark

[2] FLSmidth USA Inc., 7158 S. FLSmidth Drive, Midvale, UT 84047 USA

Title:

Electron microscope investigations of activated chalcopyrite particles via the FLSmidth® ROL Process

Author affiliations and addresses:

Adam Paul Karcz Danmarks Tekniske Universitet Dept. of Chemical and Biochemical Engineering Søltofts Plads 229 2800 Kongens Lyngby, Denmark adkr@kt.dtu.dk	Anne Juul Damø Danmarks Tekniske Universitet Dept. of Chemical and Biochemical Engineering Søltofts Plads 229 2800 Kongens Lyngby, Denmark ajp@kt.dtu.dk
Jytte Boll Illerup Danmarks Tekniske Universitet Dept. of Chemical and Biochemical Engineering Søltofts Plads 229 2800 Kongens Lyngby, Denmark jbi@kt.dtu.dk	Sara Rocks FLSmidth USA Inc. 7158 S. FLSmidth Drive Midvale, Utah 84047 USA Sally.Rocks@flsmidth.com
Kim Dam-Johansen Danmarks Tekniske Universitet Dept. of Chemical and Biochemical Engineering Søltofts Plads 229 2800 Kongens Lyngby, Denmark kdj@kt.dtu.dk	David Chaiko FLSmidth USA Inc. 7158 S. FLSmidth Drive Midvale, Utah 84047 USA David.Chaiko@flsmidth.com

Corresponding author will be Adam Paul Karcz, and he can be reached at +45 45 24 28 30.

[*] Address correspondence to E-mail: adkr@kt.dtu.dk

ABSTRACT

Because of its unique semiconductor properties, the world's most abundant copper mineral, chalcopyrite ($CuFeS_2$), is refractory with respect to atmospheric leaching using traditional acidic ferric sulfate lixiviants. FLSmidth® has developed a novel approach manipulating lattice properties of semi-conducting minerals with the benefit of increasing chemical reactivity and dissolution kinetics. In the FLSmidth® Rapid Oxidative Leach (ROL) process, leach kinetics are still further enhanced by combining chemical and mechanical processes with the assistance of a Stirred Media Reactor. Due to the reduction in surface passivation problems associated with atmospheric leaching, this process is typically able to achieve copper recoveries exceeding 95% in 6 h. An important factor contributing to this extraordinary process performance is a mineral preconditioning step (the focus of this study), which uses between 0.1 and 5 mol percent of copper (II) to dope the lattice and thereby "activate" chalcopyrite. Since lattice restructuring can have such a dramatic influence on semiconductor reactivity, the associated physico-chemical phenomena are worth studying. In this regard, we investigate the relationship between chemical activation and deformation of the chalcopyrite crystal lattice through the use of electron microscopy. Although the activation process took only an hour and the extent of conversion was on the order of a few mol%, the lattice was found to be strained throughout the particle. This paper draws some insights into the impact of applying chemical activation as a pretreatment for mechanochemical processes.

Introduction

Due to the near-term transitioning from copper oxide heap leaching to copper sulfide processing at a large number of mine sites, there is much interest in finding a cost-effective leach process which is compatible with current hydrometallurgical process infrastructures [1]. However, successful atmospheric leaching of the world's most abundant copper mineral, chalcopyrite ($CuFeS_2$), has proven to be difficult. The semiconductor properties of this mineral contribute to its refractory nature with respect to traditional acidic ferric sulfate leaching aids [2, 3]. This behavior is believed to be related to the re-supply of holes to the reaction surface as a rate-limiting step [4]. Additional contributory factors to its refractory nature include: (1) the formation of surface-bound polysulfides, (2) an elemental sulfur product layer, and (3) a variety of electrochemically passivating intermediate species, such as $Cu_{1-x}Fe_{1-y}S_{2-z}$ [5–10].

The atmospheric oxidation of $CuFeS_2$ involves the Fe(II)/Fe(III) redox couple as the primary oxidant, as explained in the following cathodic and anodic half-cell reactions:

$$CuFeS_2 \rightarrow Cu^{2+} + Fe^{2+} + 2S^0 + 4e^- \quad (1)$$

$$4Fe^{3+} + 4e^- \rightarrow 4Fe^{2+} \quad (2)$$

The collection of crystallites that make up a chalcopyrite particle will have a range of rest potentials due to variabilities in point defect concentration, lattice dislocations, and crystallite distribution. These

variabilities will affect local reaction rates, e.g., doping-induced photocatalytic activity of $InVO_4$, [11] grain growth retardation due to dislocations in electrodeposited Cu,[12] and combustion kinetics of nanocomposite energetics [13]. Nevertheless, particle corrosion rates (i.e., Eqs. 1 & 2) will be highest when the cathodic/anodic electron flow is balanced at the interfaces between reacting crystallites. Thus, if the system starts at a moderate redox potential (i.e., 650 mV, standard hydrogen electrode, SHE), then the collective rest potential would be expected to gradually rise over time due to the preferential dissolution of those crystallites that are most thermodynamically and kinetically reactive. This effect would necessitate increasing the redox potential later in the leaching process to continue driving particle dissolution to completion.

Furthermore, the Pourbaix diagram for the Cu–Fe–S–O–H_2O system (Fig. 1) suggests that the dissolution pathway for recovery of Cu^{2+} from chalcopyrite in an acid medium is a complex process, with a variety of stable intermediate sulfides as potential reaction side products (e.g., Cu_5FeS_4, CuS, Cu_2S). Fig. 1 also implies that low pH (<4) and a redox potential higher than 400 mV (SHE) is required to dissolve copper from chalcopyrite [10, 14, 15].

A large amount of research has been performed over the past several decades with a goal to better understand the thermodynamics and electrochemistry of the reactions involved in copper sulfide leaching. From this body of work, a number of processing approaches have been developed; these include, most notably, the use of heterogeneous leach catalysts [16–19] and chemical pre-conversion of chalcopyrite to more readily leachable copper sulfide products [20–25]. Especially relevant to the understanding of chalcopyrite leaching have been studies on the surface chemistry of chalcopyrite through surface spectroscopies (e.g., x-ray photoelectron, secondary ion mass, and x-ray absorption spectroscopies) and modeling (e.g., density functional theory). For example, modeling has been able to describe favorable/low-energy surfaces of chalcopyrite [26], the predicted oxidation states [27], and insights into the role of metal deficiency on surface passivation [28].

One of the more unique approaches to improving the leach kinetics involved the mechanochemical activation of chalcopyrite ($CuFeS_2$) particles in the Sherritt-Cominco process [9]. Their method focused on particle size reduction to achieve a P_{80} below 15 μm for the purpose of shortening the diffusion pathway through the particle. Their main reaction followed the form:

$$CuFeS_2 + CuSO_4 \rightarrow 2CuS + FeSO_4, \quad (3a)$$

which was performed at temperatures >150°C. Another reaction occurred for the bornite present in the concentrate, which was more desirable as a high-copper mineral:

$$Cu_5FeS_4 + CuSO_4 \rightarrow 2Cu_2S + 2CuS + FeSO_4. \quad (4)$$

However, this process also suffered from an undesirable reaction that increased the amount of copper sulfate needed for the recycle by 20-30%:

$$5CuS + 3CuSO_4 + 4H_2O \rightarrow 2Cu_2S + 4H_2SO_4. \quad (5)$$

Furthermore, at the elevated temperatures they experience more copper sulfate consumption with the covellite (CuS) product through Eqs. (3) and (4):

$$6CuS + 3CuSO_4 + H_2O \rightarrow Cu_9S_6 + 4H_2SO_4. \quad (6)$$

To prevent this from happening, Swinkels and Berezowsky introduce dissolved oxygen into the acidic solution to convert the sulfides into elemental sulfur through the following reactions:

$$Cu_2S + 2H_2SO_4 + O_2 \rightarrow 2CuSO_4 + S^0 + 2H_2O \quad (7)$$

and

$$CuS + H_2SO_4 + O_2 \rightarrow CuSO_4 + S^0 + H_2O. \quad (8)$$

An oxygen partial pressure of 1.4 kg/cm^2 was found to be adequate for Fe^{3+} oxidation, but a range of 3.5–7.0 kg/cm^2 was preferred. As can be seen, this process was very energy intensive, since it required very high temperatures (above the boiling point of water) and a large supply of oxygen to prevent parasitic side reactions. FLSmidth has developed a novel two-step approach for the atmospheric leaching of copper sulfides which uses (1) a pretreatment step utilizing chemical activation and (2) a downstream mechanochemical leaching step, which together alter lattice strain and thereby increase chemical reactivity [29, 30]. This method, drawing inspiration from other mechanochemical leaching activities [31–33], introduces additional copper (e.g., a few mol%) into the chalcopyrite crystal lattice to form non-stoichiometric Cu_xS_y compounds and is accomplished by drastically limiting the extent of reaction during the copper metathesis of chalcopyrite to covellite (CuS):

$$CuFeS_2 + Cu^{2+} \rightarrow Fe^{2+} + 2CuS \quad (9)$$

Through the use of chemical activation described above and the combination of grinding and leaching during the subsequent mechanochemical ROL process, the mechanism for dissolution becomes less influenced by electrochemical effects, and corrosion becomes seemingly insensitive to the surface passivation conditions [29]. In continuous pilot testing, copper doping of less than 0.5 mol% has significantly increased leach kinetics and copper recoveries [30, 34]. The lattice doping due to the chemical preconditioning/activation process will be the focus of the present study.

Materials and methods

Chalcopyrite was doped with 4 mol% copper as follows. A museum-grade chalcopyrite ($CuFeS_2$, Excalibur Minerals, USA) sample was ground to minus 635 mesh (less than 20 μm in diameter) using a ring and puck mill (BICO, USA). A stirred beaker was filled with deionized water (200 mL), adjusted between pH 1.0 and 4.0 with sulfuric acid, and heated to 80 °C. Copper sulfate pentahydrate ($CuSO_4 \cdot 5H_2O$, 4.08 g, Alfa, USA) and ferrous sulfate heptahydrate ($FeSO_4 \cdot 7H_2O$, 1.99 g, Alfa, USA) were added and the solution pH maintained between 2.0 and 4.0. Finely ground chalcopyrite (75.0 g)

was added to the solution to initiate the conversion reaction. The redox potential and pH were recorded throughout the process. Samples were taken during the course of the reaction, which proceeded for an hour.

Powder X-ray diffraction (XRD) measurements on planetary ball-milled (Pulverisette 6, 100 min with polished agate media) chalcopyrite particles, using a Huber G670 with 10 min exposure, were used to compare between non-activated and activated samples. The purity of the museum-grade chalcopyrite was consequently verified with XRD.

Transmission electron microscopy (TEM) samples were prepared with gallium-focused ion beam milling in a Helios NanoLab DualBeam 600 with a scanning electron microscope (SEM, see Fig. 2a-c). Platinum was deposited onto a chalcopyrite particle (stoichiometric ratio confirmed with X-ray energy dispersive spectrometry) for transfer purposes. It was milled initially at 30 kV for bulk removal around the slice before it was transferred next to a TEM grid and attached with additional platinum deposition. The final thinning involved fine milling to sub-100 nm thickness at 5 kV in order to reduce beam damage.

TEM characterization was performed with a Tecnai T20 G2 operating at 200 kV accelerating voltage. Beam alignments and astigmatism corrections were performed, and the TEM was calibrated using the ring diffraction pattern of the platinum deposited during ion milling. The pattern was found to match that of XRD reference values for platinum (see Online Resource 1).

Results and discussion

A previous study on activated chalcopyrite by Chaiko, et al. [30], found that low-conversion metathesis reactions do indeed alter the crystal lattice well beyond the local reaction site. This interesting phenomenom is the primary focus of the current investigation. Diffraction data were initially gathered using XRD (Fig. 3) to see whether it is possible to detect any differences resulting from the chemical activation (i.e., presence of new peaks). However, a maximum of 4 mol% conversion was too low to show a measurable effect on the bulk lattice properties. To better probe changes in lattice properties, more precise analytical techniques such as TEM were employed.

TEM images of some areas of interest were taken in bright field mode, wherein select area electron diffraction (SAED) was performed in distinctive regions. This can be seen best in Fig. 4, where two types of regions in the activated samples are apparent. The main features to note are regions that appear to be either polycrystalline (as in the upper part of Fig. 4a) or close to single crystalline (as in the lower two parts of Fig. 4a, labeled crystals A and B), since some twinning is commonly observed in natural chalcopyrite [35]. Indeed, these two regions showed significant differences when their diffraction patterns were compared.

Although the possibility of a difference between crystals A and B of the sample in Fig. 4 was considered, the d-spacings calculated from their diffraction patters proved that these were instead different

crystallographic orientations of the chalcopyrite lattice. These patterns were analyzed according to two different methods that produced nearly identical results. The first method involved transforming the diffraction spots into a radial distribution profile (see Fig. 5). Peak fitting was then utilized to determine the major peaks of each profile (Table 1). Based on the analysis, it was possible to determine that there was peak overlap between the two chalcopyrite regions (e.g., crystals A and B in Fig. 4); however, their intensities were of different strengths as a result of diffraction along separate zone axes.

An important discovery made evident from diffraction pattern analysis is that the d-spacings from the activated and non-activated regions are heavily altered. This effect was anticipated since the activated regions are partially converted to a complex copper sulfide, as evidenced from previous work by Chaiko, et al. [30], as well as verification of reaction kinetics of the activation step via chemical Eq. 3 (see Online Resource 2). However, it was surprising to find that the regions which are seemingly non-activated also show very different d-spacings relative to that of chalcopyrite. In that study, the d-spacings prior to activation were in agreement with reference data obtained during the XRD analysis.

The other method of analysis utilized the software CrysTBox [36, 37] to fit the collected diffraction patterns with reference data. A few examples of the fitting performed can be seen in Figs. 6, 7, and 8 and Tables 2 and 3.

In the case of chalcopyrite crystals A and B, which had only a few crystallites displaying diffraction spots, it was easy to perform the fitting using the diffraction fitting toolkit (see Fig. 6). Because the reaction product during activation was anticipated to be covellite-like in structure (Eq. 9), covellite reference data were employed. However, using the covellite reference pattern as a model produced a poor fit and led to lattice vectors in forbidden planes. Although there was more than one crystal to fit, it was possible to focus on one set of crystal diffraction spots. By assigning each spot to a lattice plane (Fig. 6b), the fitting determined the zone axis of crystal A as [0 -2 1]. Similarly, the zone axis of crystal B was determined to be [1 -1 0], which supports our earlier conclusion that the radial intensity peak differences were due to different crystal orientations. The validity of the lattice plane identification can be drawn from the associated Fig. 7. Indeed, the diffraction spot intensities for the fitting of lattice vectors A, B, and D (from Table 2) to their identified planes also carry a similar ratio of spot sizes for both the pattern and simulation.

In the case of the polycrystalline and presumably activated region, where the electron diffraction pattern shows a larger degree of poly-crystallinity, a ring fitting procedure (Fig. 8 and Table 3) typically used for amorphous materials was attempted. In this region, chalcopyrite reference data did not match the SAED pattern, so a fit with covellite was attempted instead. Although there are questions as to the reliability of the Miller indices of Fig. 7, since these are forbidden planes in the crystal lattice, the diffraction data did match a number of d-spacings associated with covellite better than it did the chalcopyrite reference pattern. This shows that the activated region is altered to be covellite-like, and this

lattice alteration can be clearly identified using diffraction imaging with TEM, where powder XRD is insufficiently sensitive to the few mol% conversion.

It should be once again noted that the d-spacings calculated with the radial distribution profile and lattice fitting uncovered similar deviations from reference data. Although the fitting was capable of identifying lattice planes and the zone axis, the values for the d-spacings show that there is significant lattice strain induced throughout the particle by lattice doping. Of great interest are the large d-spacing values which are observed in the crystalline chalcopyrite regions and are consistently greater than the expected value (3.04 Å for the [1 1 2] d-spacing, 1.85 Å for [0 2 4], and 2.65 Å for [2 0 0]). It should be noted that ion-milling has an effect of increasing the lattice spacing at the [1 1 2] plane even in pure chalcopyrite, but no such effect on other planes (see Online Resource 3). A possible conclusion is that atoms in the lattice are sitting at larger distances from each other, leading to a lower atom density. Despite having been milled to a thickness of less than 100 nm, the chalcopyrite particles observed are strained, suggesting that the native doped particles may be under even further strain.

Such effects may be an important contributing factor that play key roles in promoting the improved kinetics of the activated particles within the mechanochemical leaching system. Lattice deformations in solids have been clearly shown to affect chemical kinetics and transport phenomena [38, 39], and natural chalcopyrite has been observed to accommodate its structure to other lattices [35]. One would expect that the induced lattice strain might reduce the activation energy required for copper dissolution, and, secondly, that the particles may be more easily broken up during mechanical action in the Stirred Media Reactor (SMRt). Although the effects of the activation reaction on electrochemical properties have yet to be determined, the disruption in the lattice provides important insight into one of the main mechanisms for improved copper leaching in the ROL process. Supplementation with modeling would help to better elucidate the lattice activation mechanism.

Conclusions

In this study, it was found that the chemical activation (i.e., lattice doping with only a few mol % conversion) of chalcopyrite particles has a significant effect on the crystal structure. In the regions where the activation reaction was clearly evidenced through TEM as a polycrystalline phase, the diffraction patterns revealed a lattice that more closely resembled covellite than chalcopyrite, indicating an intermediate phase between the two. Regions of the particle, though characterized with only a few crystallites, had diffractions that resembled chalcopyrite lattice planes, but showed altered d-spacings (either equal to or larger than expected), indicating that the extent of activation reaches beyond the reacted regions.

It is likely that the lattice of chalcopyrite has been stressed by the heavy doping process (e.g., about 4 mol% conversion) to the point that particles readily relieve lattice strain by breaking apart during ion milling. After the stress has been released, the lattice partially relaxes to a more energetically favorable structure but still retains larger-than-expected d-spacings, which are not visible by XRD. Rather than

relaxing to the expected lattice parameters of unmodified chalcopyrite, these activated particles remain in this new mixed covellite-chalcopyrite state, which remains stable over at least several months. This could, at least partly, explain the improved leaching kinetics during the mechanochemical ROL process.

Additionally, the possibility that altered electrochemical properties influence leach kinetics still needs to be addressed. In particular, we aim to explain how the structural changes, arising from the activated chalcopyrite crystallites, reflect on the flow of electrons and corresponding changes in the redox potential during leaching. Future efforts will focus on characterization of the electronic structure of these activated particles. However, the implications point toward an activation process that can make significant changes to the properties of the host material through a relatively simple modification procedure and only a small amount of doping via a solution-based method. In the future, we hope to elucidate further the effects of activation through surface spectroscopy studies and computational modeling.

Acknowledgements

Acknowledgements are made for FLSmidth and Innovation Fund Denmark for their support and funding (Grant No. 39-2013-2). Additionally, thanks are given to Zoltan Imre Balogh and Jakob Birkedal Wagner from the Center for Electron Nanoscopy at the Technical University of Denmark, Kgs. Lyngby, Denmark, for help in performing FIB-SEM and interpreting diffraction results, respectively.

Conflicts of interest

The authors declare that all relationships and interests of those involved in the manuscript do not have any conflicts which could potentially influence or bias the submitted work.

Electronic supplementary information

Below is the link to the electronic supplementary material. Online resource 1 includes a report of the ring diffraction analysis used to confirm the correct calibration of the TEM. Online resource 2 provides information on the kinetics of the activation reactionanalyzed from inductively coupled plasma mass spectrometry (ICP-MS). Online resource 3 serves as a controlfor the TEM diffraction analysis since it provides details on pure chalcopyrite for comparison. (DOCX2460 kb)

References

1. Eyzaguirre C, Rocks SS, Klepper R et al (2015) The FLSmidth ® Rapid Oxidative Leach (ROL) Process: A Mechano-Chemical Approach for Rapid Metal Sulfide Dissolution. In: Hydroprocess, Proceedings of the 7th international seminar on process hydrometallurgy, Antofagasta, Chile, pp 1–11

2. Majima H, Awakura Y, Hirato T, Tanaka T (1985) The Leaching of Chalcopyrite in Ferric Chloride and Ferric Sulfate Solutions. Can Metall Q 24:283–291. doi: 10.1179/cmq.1985.24.4.283

3. Osseo-Asare K (1992) Semiconductor electrochemistry and hydrometallurgical dissolution processes. Hydrometallurgy 29:61–90. doi: 10.1016/0304-386X(92)90006-L

4. Crundwell FK (2015) The semiconductor mechanism of dissolution and the pseudo-passivation of chalcopyrite. Can Metall Q 54:279–288. doi: 10.1179/1879139515Y.0000000007

5. Dutrizac JE (1981) The dissolution of chalcopyrite in ferric sulfate and ferric chloride media. Metall Trans B 12:371–378. doi: 10.1007/BF02654471

6. Ghahremaninezhad A, Asselin E, Dixon DG (2010) Electrochemical evaluation of the surface of chalcopyrite during dissolution in sulfuric acid solution. Electrochim Acta 55:5041–5056. doi: 10.1016/j.electacta.2010.03.052

7. Mehta AP, Murr LE (1983) Fundamental studies of the contribution of galvanic interaction to acid-bacterial leaching of mixed metal sulfides. Hydrometallurgy 9:235–256. doi: 10.1016/0304-386X(83)90025-7

8. Munoz PB, Miller JD, Wadsworth ME (1979) Reaction Mechanism for the Acid Ferric Sulfate Leaching of Chalcopyrite. Metall Mater Trans B 10B:149–158.

9. Swinkels GM, Berezowsky RMGS (1978) Swinkels 1978 – The Sherrit-Cominco Copper Process – Part 1. CIM Bull 71:105–121.

10. Córdoba EM, Muñoz JA, Blázquez ML, et al (2008) Leaching of chalcopyrite with ferric ion. Part IV: The role of redox potential in the presence of mesophilic and thermophilic bacteria. Hydrometallurgy 93:106–115. doi: 10.1016/j.hydromet.2007.11.005

11. Rakesh K, Khaire S, Bhange D, et al (2011) Role of doping-induced photochemical and microstructural properties in the photocatalytic activity of InVO4 for splitting of water. J Mater Sci 46:5466–5476. doi: 10.1007/s10853-011-5489-5

12. Jung K, Conrad H (2007) Retardation of grain growth in electrodeposited Cu by an electric field. J Mater Sci 42:3994–4003. doi: 10.1007/s10853-006-0177-6

13. Dreizin EL, Schoenitz M (2017) Mechanochemically prepared reactive and energetic materials: a review. J Mater Sci 1–21. doi: 10.1007/s10853-017-0912-1

14. Garrels RM, Christ CL (1965) Solutions, minerals and equilibria, 1st Ed. Harper & Row, New York

15. Schlesinger ME, Biswas AK (2011) Extractive metallurgy of copper, 5th Ed. Elsevier, Oxford

16. Dixon DG, Rivera-Vasquez B (2012) Leaching process for copper concentrates containing chalcopyrite. US 8,968,442 B2. 1–15.

17. Dixon DG, Nazari GT (2014) Leaching process for copper concentrates containing chalcopyrite. US 8,795,612 B2. 1–16

18. Miller JD, McDonough PJ, Portillo HQ (1981) Electrochemistry in silver catalysed ferric sulfate leaching of chalcopyrite. In: Kuhn MC (ed) Process and fundamental considerations of selected hydrometallurgical systems. SME-AIME, New York, pp 327–338

19. Wan RY, Miller JD, Simkovich G (1985) Enhanced ferric sulfate leaching of copper from CuFeS2 and C particulate aggregates. In: Proceedings of MINTEK 50 international conference on mineral science and technology, Council for Mineral Technology, Sandton, South Africa, pp 575–588

20. Baczek FA, Wojcik BC, Jueschke AA et al (1981) Recovering copper from chalcopyrite concentrate. US 4,256,553. 1–12

21. Peters E, Hackl R (1984) Iron-copper separation by reduction leaching. CA 1,179,509. 1–42

22. Sohn H-J, Wadsworth ME (1984) Chemical conversion of chalcopyrite to copper sulfides. In: SME-AIME Annual Meet. Society of Mining Engineers of AIME, Los Angeles,CA, pp 1–11

23. Padilla R, Olivares E, Ruiz MC, Sohn HY (2003) Kinetics of the sulfidation of chalcopyrite with gaseous sulfur. Metall Mater Trans B 34:61–68. doi: 10.1007/s11663-003-0055-4

24. Collier DE, Ring RJ, Wedderburn BJ et al (2004) Process of upgrading a copper concentrate. WO 2,004,106,561 A1.1–14

25. Peterson RD, Wadsworth ME (1994) Solid, solution reac-tions in the hydrothermal enrichment of chalcopyrite atelevated temperatures. In: EPD Congress 1994. The Miner-als, Metals & Materials Society, pp 275–291

26. Chen VH-Y, Mallia G, Martinez-Casado R, Harrison NM(2015) Surface morphology of CuFeS2: the stability of thepolar (112)/(112) surface pair. Phys Rev B 92:155426.doi:10.1103/ PhysRevB.92.155426

27. Wang J, Gan X, Zhao H et al (2016) Dissolution and passivation mechanisms of chalcopyrite during bioleaching: DFT calculation, XPS and electrochemistry analysis. Miner Eng 98:264–278. doi:10.1016/j.mineng.2016.09.008

28. Yang Y, Harmer S, Chen M (2015) Synchrotron-based XPS and NEXAFS study of surface chemical species during electrochemical oxidation of chalcopyrite. Hydrometallurgy 156:89–98. doi: 10.1016/j.hydromet.2015.05.011

29. Chaiko D, Baczek FA, Rocks SS, et al (2015) The FLS rapid oxidative leach (ROL) process . Part I : mechano-chemical process for treating chalcopyrite. In: Conf. Metall. The Conference of Metallurgists, Toronto, Ontario, pp 1–11

30. Chaiko D, Rocks SS, Walters T, et al (2015) The FLS rapid oxidative leach (ROL) process . Part II : a new chemical activation process for chalcopyrite. In: Conf. Metall. The Conference of Metallurgists, Toronto, Ontario, pp 1–15

31. Cobble JR, Jordan CE, Rice DA (1993) Hydrometallurgical production of copper from flotation concentrates. USBM RI 9472. 1–20.

32. Baláž P, Achimovičová M (2006) Mechano-chemical leaching in hydrometallurgy of complex

sulphides. Hydrometallurgy 84:60–68. doi: 10.1016/j.hydromet.2006.04.006

33. Baláž P (2004) Mechanochemistry of sulphides. J Mater Sci 39:5097–5102. doi: 10.1023/B:JMSC.0000039190.72325.cf

34. Mulligan M, Chaiko D, Baczek FA et al (2016) TheFLSmidthÒrapid oxidative leach (ROL) process: a mechano-chemical approach and industry applications for rapid metal sulfide dissolution. In: Hydrometallurgy conference, sustainable hydrometallurgical extraction of metals, Cape Town, South Africa, pp 1–11

35. Murr LE, Lerner SL (1977) Transmission electron microscopic study of defect structure in natural chalcopyrite (CuFeS2). J Mater Sci 12:1349–1354. doi: 10.1007/BF00540848

36. Klinger M, Jäger A (2015) Crystallographic Tool Box (CrysTBox): automated tools for transmission electron microscopists and crystallographers. J Appl Crystallogr 48:2012–2018. doi: 10.1107/S1600576715017252

37. Klinger M, Němec M, Polívka L, et al (2015) Automated CBED processing: sample thickness estimation based on analysis of zone-axis CBED pattern. Ultramicroscopy 150:88–95. doi: http://dx.doi.org/10.1016/j.ultramic.2014.12.006

38. Tovbin YK (2007) Atomic-Molecular Kinetic Theory of Physico-Chemical Processes in Condensed Phase and Interfaces. Thin Film Nanostruct 34:347–464. doi: 10.1016/ S1079-4050(06)34008-2

39. Gabidullin RM (1977) Effect of dislocations on kinetics of metal degassing. Sov Mater Sci 12:42–45. doi: 10.1007/BF00728377

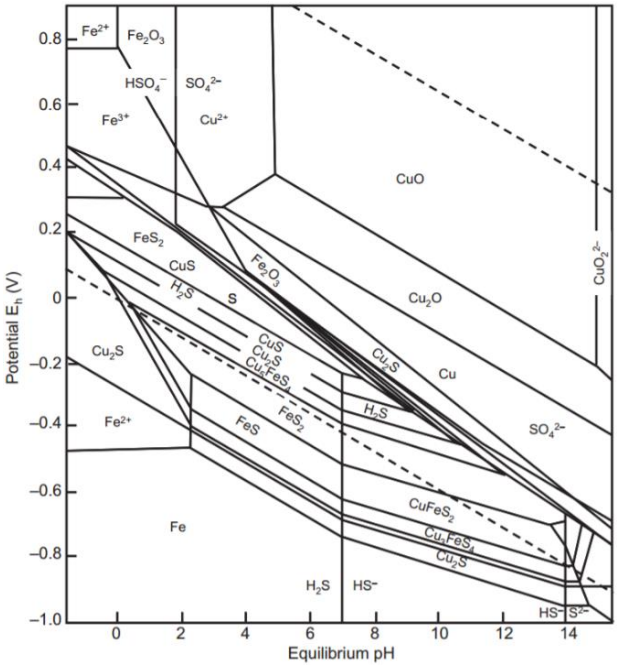

Figure 1 Pourbaix diagram for the Cu-Fe-S-O-H_2O system at 25°C. [Cu] = 0.01 M, [Fe] = [S] = 0.1 M. Reproduced with permission from Elsevier.[12][1]

[1] Reprinted from Extractive Metallurgy of Copper, 5th edition, Schlesinger ME, Biswas AK, Chapter 15 - Hydrometallurgical Copper Extraction: Introduction and Leaching, Pages 281-322, Copyright 2011, with permission from Elsevier.

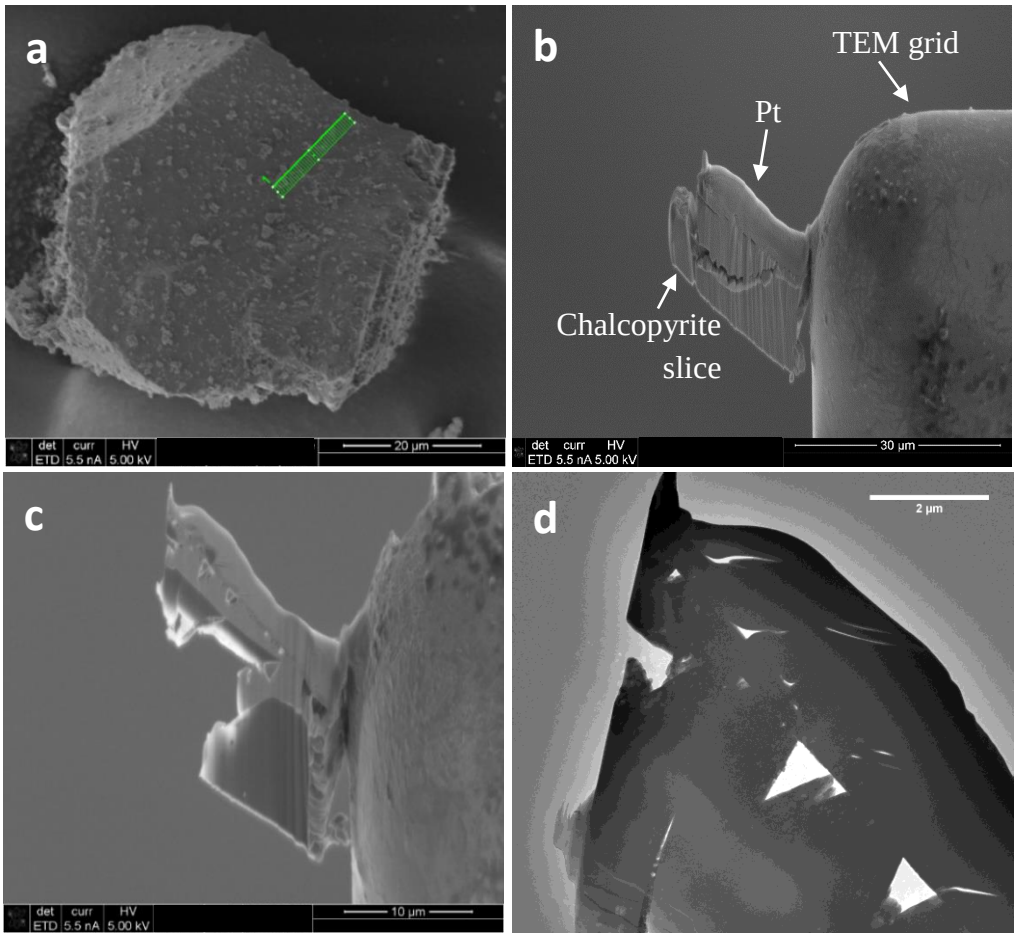

Figure 2 a SEM image of a chalcopyrite particle examined in this study with green rectangular area marked "1" where platinum was to be deposited. **b** The slice viewed in SEM from the side after course milling with the focused ion beam at 30 kV and attachment to a TEM grid on the right. The chalcopyrite portion of the sample is more easily distinguished visually with the presence of striations. The platinum deposited on top of the particle is labeled "Pt deposit." **c** SEM image of the same slice after further thinning at 5 kV to less than 100 nm thickness. As can be seen, portions of the slice have broken off as it became thinner. **d** TEM image of the top portion of the same slice from Fig. 2c which was used for some of the diffraction studies.

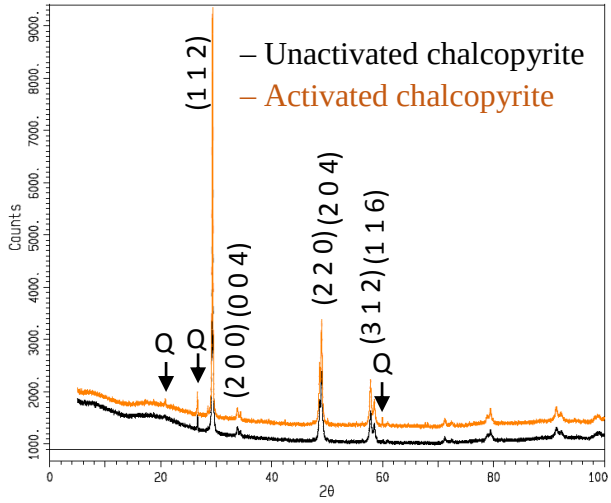

Figure 3 XRD patterns of the chalcopyrite powders with and without activation. The activated sample has a few additional minor peaks, which are due to quartz impurities (labeled Q). First seven major peaks of chalcopyrite are presented (AMCSD 0018622).

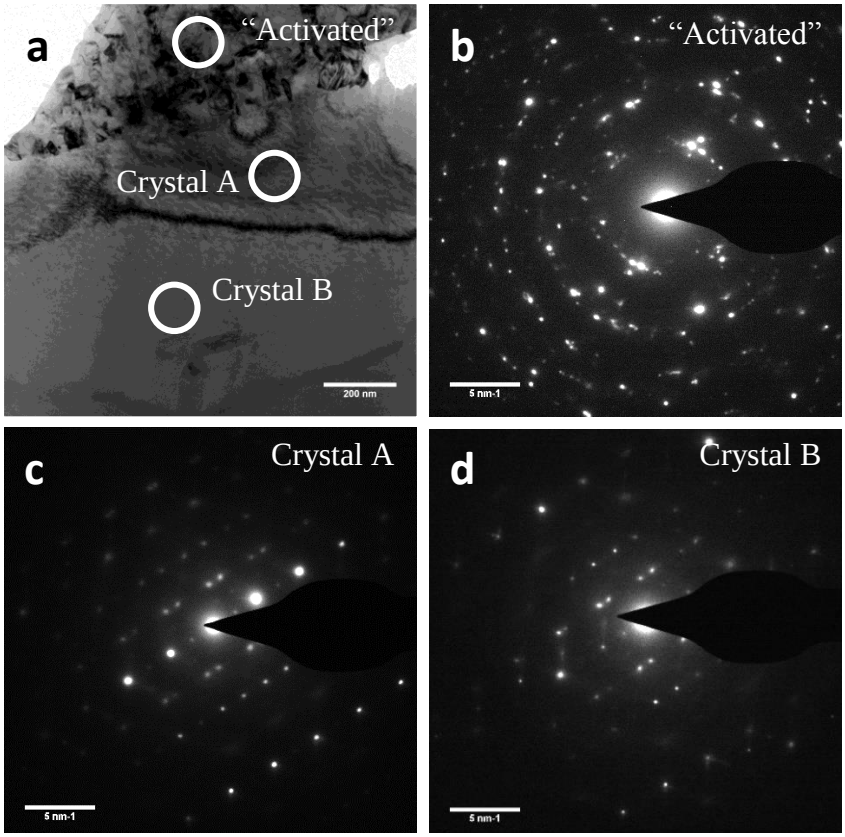

Figure 4 a TEM image of the area over which the following diffraction patterns were taken. Circles on the image indicate the corresponding diffraction patterns to follow. **b** SAED pattern which is referred by the upper circle in the previous image and within a polycrystalline, presumably activated region. **c** SAED pattern which is referred by the middle circle and corresponds to a possible chalcopyrite region (denoted "crystal A"). **d** SAED pattern corresponding to a bulk chalcopyrite region, which is referred by the lower circle (denoted "crystal B"). Twinning was observed in **c** and **d**.

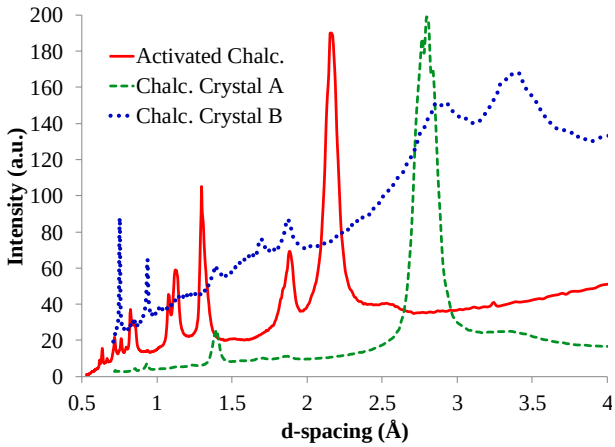

Figure 5 The radial distribution profile of the three SAED locations in Fig. 4.

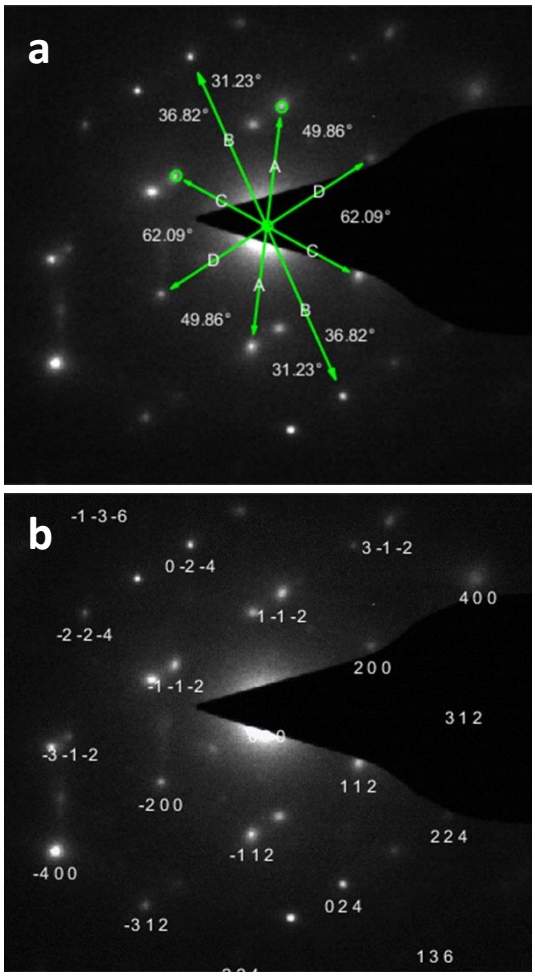

Figure 6 Fitting report with chalcopyrite reference data (AMCSD 0018623) for the chalcopyrite crystal A. **a** Lattice vector quantification after spot matching. **b** Zone axis was calculated to be [0 -2 1] from vectors above.

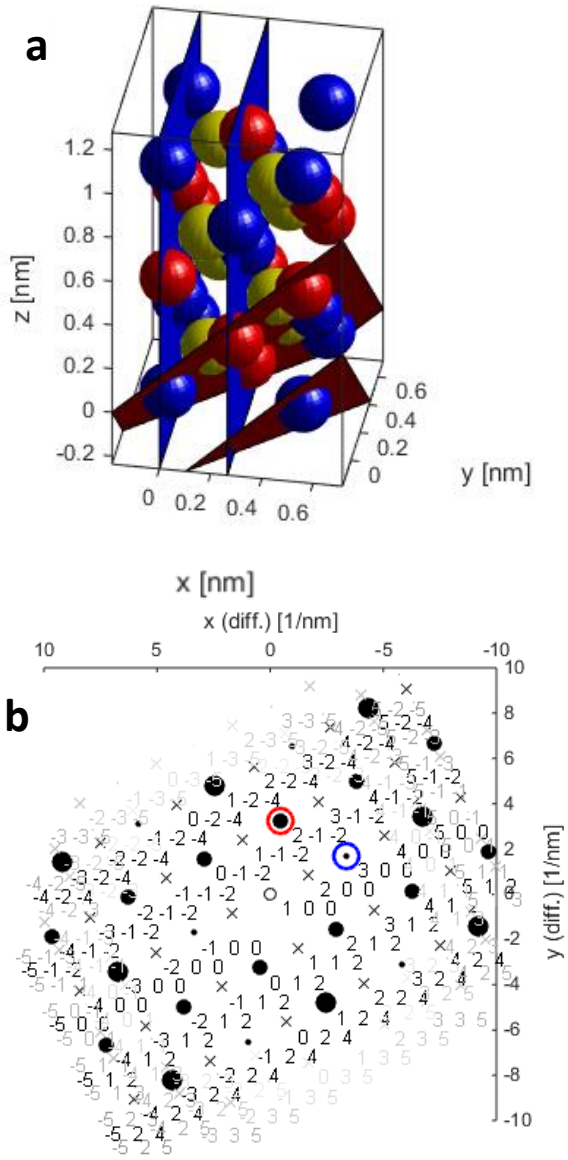

Figure 7 a Unit cell generated using chalcopyrite reference data (AMCSD 0018623) and the [1 -1 -2] and [2 0 0] lattice planes (blue on right and red on left, respectively). The atoms are as follows: iron in red, copper in blue, and sulfur in yellow. **b** The simulated diffraction pattern of **Fig. 6** SAED along the [0 -2 1] zone axis with highlighting of the two planes (same color coding for planes). Note the similar ratio of beam spot sizes with **Fig 6b**.

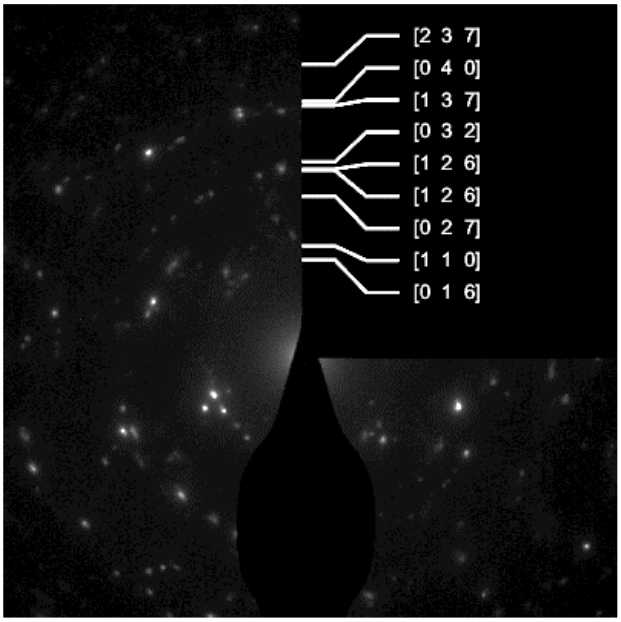

Figure 8 Ring pattern fitting against covellite reference data (AMCSD 0000534) for the polycrystalline activated region.

Table 1 Summary of averaged peaks (in units of Å) from Fig. 5. Reference X-ray diffraction peaks are shown where applicable (AMCSD 0018623 for chalcopyrite and 0000534 for covellite).

Non-activated	Activated	Ref. Data	Candidate
3.353			
	3.254	3.221	Cov.
	3.020	3.048	Cov.
2.852		2.813	Cov.
	2.559	2.605	Chalc.
2.164			
	2.011		
1.989			
	1.919	1.903	Cov.
1.871	1.876	1.868	Chalc.
	1.715	1.735	Cov.
1.693			
1.546		1.575	Chalc.
1.394	1.397	1.391	Cov.
	1.324	1.344	Cov.
1.254			
	1.201	1.212	Cov.
1.143			
	1.128		Cov.

Table 2 Summary of d-spacings and lattice planes from Fig. 6.

	d-spacing		Vector identification
	[Å]	[1/nm]	
A	2.9002	3.4481	1 -1 -2
B	1.8739	5.3364	0 -2 -4
C	3.3524	2.9829	-1 -1 -2
D	2.7633	3.6189	-2 0 0

Table 3 Summary report of associated **Fig. 7**.

Ring identification				
Plane	Radius [1/nm]		d-spacing [Å]	
	theor.	measured	theor.	measured
[2 3 7]	13.941	13.925	0.72	0.72
[0 4 0]	12.175	12.155	0.82	0.82
[1 3 7]	11.78	11.956	0.85	0.84
[0 3 2]	9.213	9.274	1.09	1.08
[1 2 6]	8.85	8.931	1.13	1.12
[1 2 6]	8.85	8.874	1.13	1.13
[0 2 7]	7.443	7.647	1.34	1.31
[1 1 0]	5.272	5.279	1.90	1.89
[0 1 6]	4.769	4.622	2.10	2.16